Phase contrast imaging interferometer for edge density fluctuation measurements on LHD

K. Tanaka[a)]
National Institute for Fusion Science, 322-6 Oroshi-Cho, Toki-City, Gifu-Ken, Gif 509-5952, Japan

L. N. Vyacheslavov
Budker Institute of Nuclear Physics, 630090 Novosibirsk, Russia

T. Akiyama
Tokyo Institute of Technology, Meguro-ku, Tokyo 152-8550, Japan

A. Sanin, K. Kawahata, T. Tokuzawa, and Y. Ito
National Institute for Fusion Science, 322-6 Oroshi-Cho, Toki-City, Gifu-Ken, Gif 509-5292, Japan

S. Tsuji-Iio
Tokyo Institute of Technology, Meguro-ku, Tokyo 152-8550, Japan

S. Okajma
Chubu University, Kasugai 487-8501, Japan

(Presented on 8 July 2002)

A phase contrast interferometer employing a CO_2 laser (wavelength $\lambda_i = 10.6\,\mu$m) is designed and installed in order to study density fluctuations on a large helical device. A 250×50 mm slab beam passes the edge of the plasma, where $\rho = r/a > 0.65$, and provides observations of edge density fluctuations. A spatial image of the integrated fluctuations is measured by a multichannel detector array, of which the effective spacing is 5 mm in the plasma. Measured wave number components are dominated by radial components, and within the range of $7.2\times10^{-2} \leqslant k \leqslant 0.63\,\mathrm{mm}^{-1}$ and within the frequency range of 5–125 kHz. A clear difference in the fluctuation levels and peak wave numbers are observed between different discharges, which differ in the energy confinement. © *2003 American Institute of Physics.* [DOI: 10.1063/1.1538361]

I. INTRODUCTION

Microturbulence is one of the most important physical quantities, which determines the anomalous transport. Turbulent electron-density fluctuations can induce enhanced particle and energy flux.[1] A phase contrast interferometer (PCI) is installed on a large helical device (LHD) for the measurement of the microturbulent electron-density fluctuations in order to study anomalous transport. PCI is a powerful diagnostic for observing electron-density fluctuations. It records small phase variations of the probing beam produced by the electron-density fluctuations as small intensity variations. This becomes possible by using a homodyne scheme giving a $\pi/2$ initial phase difference between the scattered and nonscattered components of the laser radiation. Since PCI employs a homodyne scheme with an internal reference beam, a phase counter and digital phase analysis technique is not necessary, therefore fine phase resolution is possible, which cannot be achieved by using a conventional heterodyne interferometer. Also, PCI is capable of measuring a wide range of wave-number measurements. PCI was installed on the TCA tokamak [2] and later on Heliotron E[3,4] and DIII-D.[5,6]

II. PRINCIPLE OF PCI

Figure 1 shows a schematic view of a PCI. The plane wave front of the incident laser beam is modulated in phase by the change of the refractive index due to electron-density fluctuations in the plasma. Here, let the electric field of the incident wave be

$$E_0 = Ae^{i(\omega t + kz)}. \tag{1}$$

Then, the phase modulated beam is

$$E_1 = E_0 e^{i\phi(x,t)}, \tag{2}$$

where $\phi(x,t)$ is the modulated phase.

The positive and negative first-order scattered components appear due to the Raman-Nath diffraction[7] for the typical amplitude and wave number of fluctuations in magnetically confined plasmas with the use of a 10.6 μm CO_2 laser beam. A simple optical system can give an image of the modulated wave front in the image plane as shown in Fig. 1. In principle, from this phase image, fluctuation in the object plane can be observed by using phase measurements in the image plane. This diagnostic can possibly use a far infrared radiation (wavelength 0.1–1 mm) as a source of the probe beam. However, on LHD, phase jump due to beam refraction sometimes occurs on the existing far-infrared interferometer (wavelength 118.9 μm) at high density ($\sim 1\times10^{20}\,\mathrm{m}^{-3}$). The deformation of the wave front either becomes significant due to refraction and aperture diffraction for the far-infrared beam. This affects the quality of the image of the fluctuations substantially. The use of a shorter wavelength (10.6 μm) promises a clearer image than that for a far-infrared beam. In

a)Electronic mail: ktanaka@ms.nifs.ac.jp

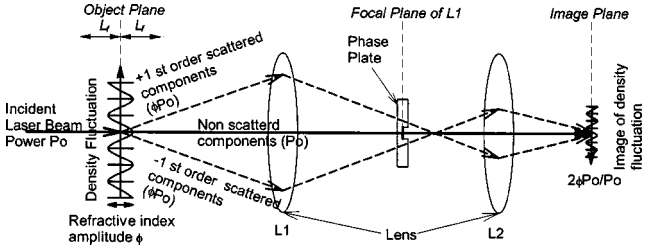

FIG. 1. Principle of the phase contrast interferometer. L_f is depth of field.

addition, scattering of 10.6 μm radiation by small-size fluctuations occurs at modest angles, that permits collecting all of the scattered radiation and the achievements of fine spatial resolution. However, there is a difficulty of the measurements using 10.6 μm. The phase modulation due to the microturbulent fluctuations by using 10.6 μm is very small $(10^{-3}-10^{-2}\,\mathrm{rad})$, so it is technically difficult to record them by using a conventional phase counter or digital phase analysis techniques and still keep good enough time resolution (1–10 μs). PCI makes this possible by using the following scheme.

As shown in Fig. 1, in PCI, a phase plate is placed in the focal plane of the lens $L1$. This phase plate is transparent and has a groove. Because of the difference in angles between scattered and nonscattered components, they are focused outside and inside the groove, respectively. The difference of the thickness of the phase plate gives the effective path difference, which is a quarter of the incident laser wavelength. Then the electric field of the beam in the imaging plane of the lens $L1$ is

$$E_2 = E_1 e^{i\phi(-x/M,t)} \approx E_1[1+i\phi(-x/M,t)] \rightarrow E_1[1+\phi(-x/M,t)], \quad (3)$$

where M is the magnification of the optical system and we dropped in Eq. (3) a quadratic phase factor produced by the optical system. Equation (3) means that small phase modulation is converted by the phase plate to amplitude modulation. Then, in the imaging plane, the intensity of the beam is

$$P = E_2 E_2^* \approx E_0^2(1+2\phi), \quad \phi \ll 1. \quad (4)$$

Phase modulation manifests itself as an intensity modulation. The measurements of the small intensity modulation are technically easier and simpler than small phase measurements. This is an advantage of PCI. More precise analytical expressions of the image with a Gaussian beam by using Fresnel-Kirchhoff diffraction integration are obtained in Ref. 8. The ratio of the first to the second term of Eq. (4) gives the absolute value of the fluctuation amplitude and promises good accuracy in the measurements.

In Fig. 1, if the fluctuation is located apart from the object plane, the image in the image plane is deformed because of defocusing. To get an image in the image plane without deformation, the distance from the object plane to the density fluctuation should be much less than $L_f = \pi k_i / k_p^2$, where L_f is the field depth, k_p is a wave number of the fluctuations, and k_i is the wave number of the incident beam.[9–11] For a plasma wave located at a distance L_f from the object plane, the amplitude component in the image of the fluctuations, which is measured by PCI, becomes zero. This means that the PCI amplitude image is converted to a phase image. For the heterodyne interferometer, respectively, the phase component in the image of the plasma wave shifted by L_f from the object plane becomes zero and the image is converted to a pure amplitude image. Some details of the transformation of the phase and amplitude components are described in Ref. 12. Recently, a technique for localized measurements along the beam axis for large k_p by using the relation between amplitude and phase components of the defocused image has been proposed.[11]

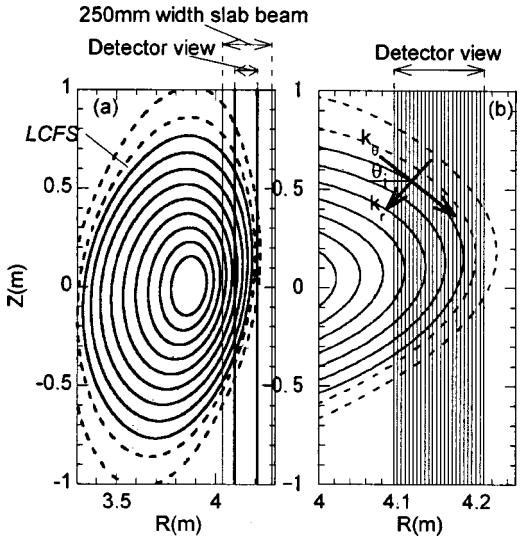

FIG. 2. (a) Measured cross section of PCI and (b) expanded views. The vertical lines indicate viewing lines of the detector array. Magnetic flux surfaces are shown from $\rho=0.1$ up to 1.2 every 0.1 step.

III. EXPERIMENTAL SETUP

The PCI system is one of the branches of CO_2 laser diagnostics on LHD and the other branches are used for the density profile measurements and vibration compensation.[13] The present 250×50 mm slab beam is vertically injected and covers a region of $\rho = r/a > 0.65$, where ρ is the normalized radial position and a is the average minor radius, as shown in Fig. 2. Figure 3 shows the detection optics of the PCI, heterodyne CO_2, and YAG laser interferometers.[13] Two off-axis parabolic mirrors and three spherical lenses are used in the imaging optics. A liquid-nitrogen-cooled 32-channel HgCdTe linear array of photoconductive detectors is employed for the signal detection. The position of the parabolic mirrors, lenses, and detector are determined in order to get an image of the center of the plasma at the detector position. Simultaneously, these positions and configurations of optical elements are optimized to minimize the effects of spherical aberration by using the software ZEMAX.[14] The effective separation of the detector elements in the plasma is 5 mm. The maximum detectable wave number is determined by the sampling theorem and it is 0.63 mm^{-1}. $L_f = 5.17$ m for $k_p = 0.63\,\mathrm{mm}^{-1}$, is much longer than the plasma size, therefore, all measurable wave-number components are uniformly integrated along the viewing line. The minimum detectable wave number is determined by the setup of the phase plate.

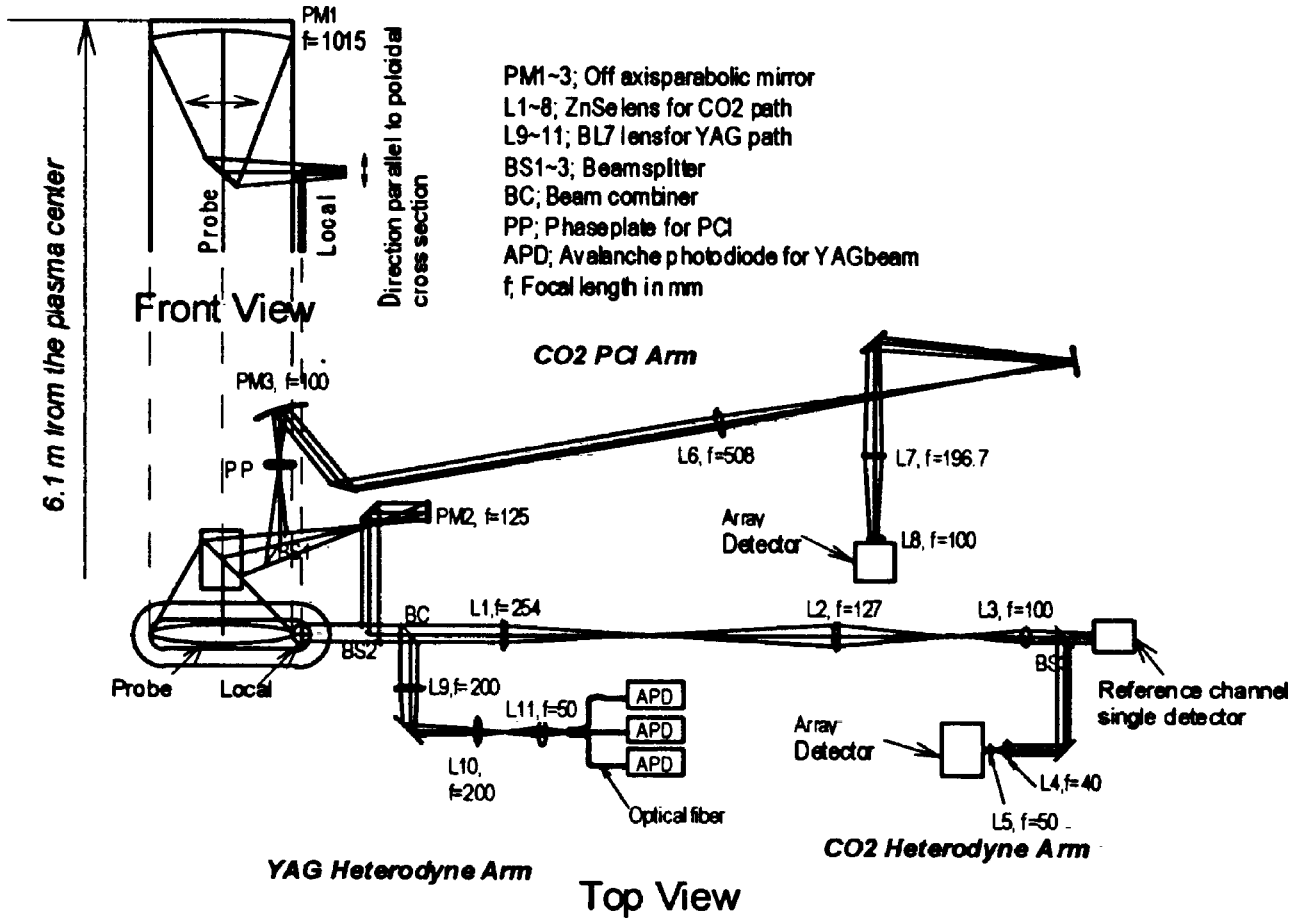

FIG. 3. Detection optics of the CO_2 laser diagnostics.

If the scattered and nonscattered components are overlapped at the phase plate, a $\pi/2$ phase difference cannot be given, and then the amplitude image cannot be obtained. These conditions are determined by the width of the groove of the phase plate and the focal spot size on the phase plate. Therefore, good focusing mirrors or lenses are the key optics of PCI as well as the phase plate. The phase plate is the same one, which was used for Heliotron E experiments.[3,4] The minimum detectable wave number is experimentally determined from the sound wave measurements and is 0.072 mm^{-1}.

In order to observe components of the fluctuations normal to the magnetic field, which play important roles in transport, the axis of array has to be adjusted to the perpendicular to the magnetic field. However, on LHD, magnetic-field lines are inclined $\pm 45°$ at ± 1 m from the equatorial plane due to the magnetic shear. Presently, the axis of the array is set to be perpendicular to the field line in the equatorial plane. Because of this inclined angle, the measured wavelength of the fluctuations traveling normally to the beam at the top and bottom plasma edges are decreased relative to real ones about 30%. Taking advantage of the field shear, scattered components corresponding to the field line can be selected by placing a slit in the focal plane. This technique provides a way to obtain the local information of plasma fluctuations along the viewing line.[15]

IV. EXPERIMENTAL RESULTS

The diffusion coefficients on LHD, which are estimated from the density modulation experiments, are anomalous ones (one order of magnitude larger than neoclassical prediction[16]), and thermal diffusion from the power balance analysis is anomalous as well.[17] Therefore, study of the microturbulence is of essential importance on LHD. In this section, fluctuation signals and spectra of the PCI from two different discharges, which have different confinement characteristics are discussed.

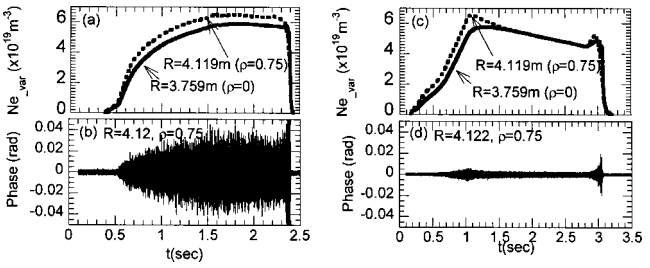

FIG. 4. (a) and (c) Time trace of the density and (b) and (d) PCI signals. (a) and (b) are at $Bt=1$ T, Hydrogen discharge (shot 34 780) and $\tau_e=36$ m s. (c) and (d) are at $Bt=2.64$ T. He discharge (shot 34 911) and $\tau_e=157$ m s. Both are NBI heated discharges at Rax (magnetic axis position) $=3.75$ m. Absorption power of NBI is 4.7 and 2 MW at 1 and 2.64 T operations, respectively.

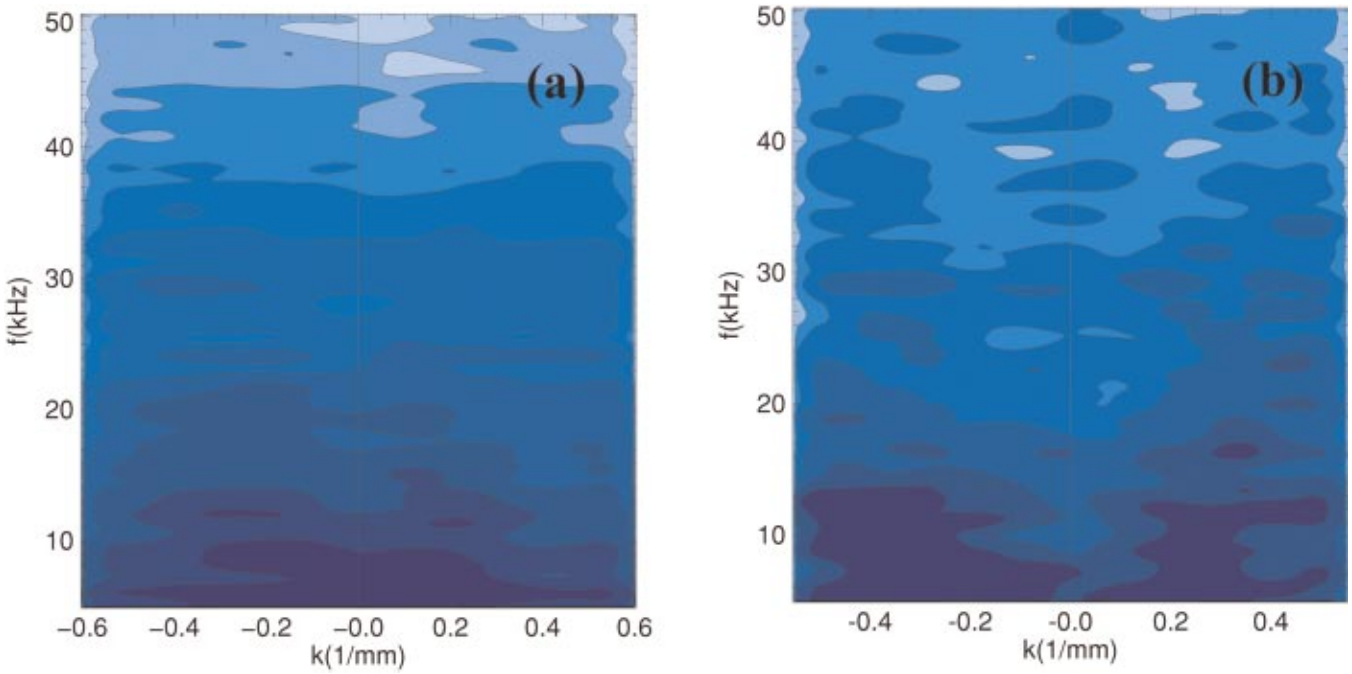

FIG. 5. (Color) $S(k,f)$ spectrum of (a) 1 T discharge and (b) 2.64 T discharge. Data are estimated from 1.5 and to 2 s. Contours of $S(k,f)$ are plotted every 3 dB. Dense color indicates stronger intensity.

Figure 4 shows density traces and PCI signals. The plasmas in these two shots are heated by neutral beam injection (NBI) at the same magnetic axis position (Rax=3.75 m) with different toroidal magnetic fields (Bt). The plasma density is almost the same in both shots, and density profiles are slightly hollow in both discharges. Therefore, the edge averaged density is slightly higher than the central one. The difference of Bt causes about a factor of 4 different energy confinement times (36 m s for 1 T operation and 153 m s for 2.64 T operation). As shown in Figs. 4(b) and 4(d), PCI signals exhibit a clear difference in the amplitude. The root mean square of the internal phase noise is determined by the detector noise, and is about 0.2 mrad. It is more than one order of magnitude lower compared with conventional phase counters at 10.6 μm.

Figure 5 shows the joint wave-number-frequency power spectrum $[S(k,f)]$. $S(k,f)$ is calculated using signals from 24 channels of a 32 channel detector array with a time interval of 1.5–2 s for both discharges. The obtained $S(k,f)$ shows a broad spectrum both in frequency and wave number. The frequency spectrum in the time domain is calculated from the signals of each channel, and the wave-number spectrum is derived by Fourier transform of the spatial distribution of the real and imaginary parts of the frequency spectrum at each frequency component. Figure 6 shows the wave-number integrated frequency spectrum and frequency integrated wave-number spectrum. The lower and upper cutoff of the detector and amplifier system is 5 and 500 kHz, respectively. Signals are acquired by 250 kHz sampling, which corresponds to a 125 kHz Nyquist frequency. However, as shown in Fig. 6(a), the dominant spectral components are lower than 50 kHz.

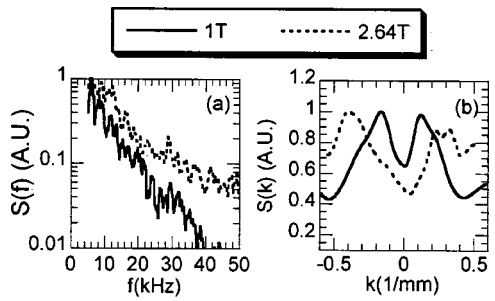

FIG. 6. (a) Wave number integrated frequency spectrum and (b) frequency integrated wave number spectrum. Data are normalized by the maximum values.

The PCI technique is sensitive to fluctuations traveling perpendicular to the beam axis. If the propagation direction of the plasma wave varies from the perpendicular to the beam axis like the poloidal propagation shown in Fig. 2(b), it means that the real wave has a considerably longer wavelength than that measured by Fourier analysis of the PCI image. Therefore, the poloidal wavelength is measured as 0–0.3 times of the real poloidal wavelength, the radial wavelength is measured as 0.95–1 times the real radial wavelength. However, this is for the case of the plane-wave model, for the more precise arguments in the case of the turbulent fluctuations, numerical modeling is necessary.[6] One of the possible interpretations of the dominant low-frequency components is that the poloidal motion projected on the perpendicular to the beam axis becomes weaker and it is less than 30% of the real poloidal motion.

The second effect is the integration of signals from the upper and lower parts of the plasma along the viewing line that can result in an almost symmetric wave-number spec-

trum shown in Fig. 6 even in case of plasma rotation in the poloidal direction. The fact that the spectral peaks are located at $k \neq 0$ argues in the case of the edge position of PCI, however, in favor of the conclusion that the observed spatial spectrum is associated more with the radial structure of the fluctuations rather than with the poloidal one.[18] There is about a 30% uncertainty of the wave numbers due to the shear effects, which is described in the previous section. However, the integration of the poloidal propagation and magnetic shear effects are the same for both discharges, therefore, the difference of the peak wave number, which is 0.15 mm^{-1} for a 1 T discharge and 0.4 mm^{-1} for a 2.64 T discharge is due to the difference of the characteristics of the fluctuations. If the step size of the diffusion process is determined by the fluctuation wavelength, the diffusion coefficients are proportional to the square of the fluctuation wavelength. The longer energy confinement time at 2.64 T operation qualitatively agrees with a larger wave number at 2.64 T compared with those of 1 T operations. It is important also that the intensity of the plasma fluctuations at 1 T is almost 1 order of magnitude higher than those at 2.64 T operation.

The amplitude of the line-averaged density fluctuations can be estimated as follows assuming fluctuations are homogeneous and isotropic. Although a more precise model taking account of the inhomogeneity and anisotropy of the wave-number spectrum is necessary for precise arguments, here, we made a rough estimation to evaluate the fluctuation level and compare them between two discharges. If one supposes a model of noncorrelated plasma waves of characteristic of wavelength λ_p and characteristic thickness along the viewing line also λ_p, then the intensity of the scattered radiation is just the intensity produced by a single wave multiplied by the number of waves L/λ_p along the beam path in the plasma L. The amplitude of the signal produced by interference of the zero order and scattered radiation is proportional to $\sqrt{L/\lambda_p}$ from a random walk argument.

As a result, the root mean square (rms) of the measured integrated signals is described by Ref. 19

$$\phi_{\mathrm{rms}} = \sqrt{\frac{L}{\lambda_p}(r_e \lambda_i \delta n_e \lambda_p)^2}, \tag{5}$$

where r_e is the electron classical radius and δn_e is the fluctuation amplitude. The phase shift due to the background plasma density is

$$\phi_0 = r_e \lambda_i \overline{n_e} L, \tag{6}$$

where $\overline{n_e}$ is the line-averaged density. From Eqs. (5) and (6), the averaged fluctuation level is given by the following:

$$\frac{\delta n_e}{\overline{n_e}} = \frac{\phi_{\mathrm{rms}}}{\phi_0}\sqrt{\frac{L}{\lambda_p}}. \tag{7}$$

From Fig. 6(b), $\lambda_p = 41.9$ mm for 1 T operation and $\lambda_p = 15.7$ mm for 2.64 T operation and the averaged root mean square between $t = 1.5-2$ s of PCI signal of Figs. 4(b) and 4(d), averaged fluctuation level at $\rho = 0.75$ is 1.98% for 1 T operation and 0.27% for 2.64 T operation. About a factor of 7 difference of fluctuation levels are obtained.

V. SUMMARY

Results of PCI on LHD are obtained. From the analysis of two discharges with different confinement conditions, clear differences of the amplitude and spectrum structure are established. However, in the present arrangements, detailed spatial profiles are impossible to acquire due to the integration effect. And interpretation of the wave-number spectrum is also complicated. For more precise interpretation of the data, local information along the beam axis is extremely essential. Several techniques (defocusing effect technique,[11] magnetic shear technique,[15] and crossed-beam technique[20]) are planned in the near future to get local information. Then, comparison with local transport coefficients by changing plasma parameter can be implemented.

[1] A. J. Wootton *et al.*, Phys. Lett. B **2(12)**, 2879 (1990).
[2] H. Weisen, CH. Hollenstein, and R. Nehn, Plasma Phys. Controlled Fusion **20**, 293 (1988).
[3] K. Tanaka *et al.*, Jpn. J. Appl. Phys., Part 1 **31**, 2260 (1992).
[4] K. Tanaka *et al.*, J. Phys. Soc. Jpn. **62**, 3092 (1993).
[5] S. Coda, M. Porkolab, and T. N. Carlstrom, Rev. Sci. Instrum. **63**, 4974 (1992).
[6] S. Coda and M. Porkolab, Rev. Sci. Instrum. **66**, 454 (1995).
[7] W. R. Klein and W. D. Cook, IEEE Trans. Sonics Ultrason. **SU-14**, 123 (1967).
[8] K. Matsuo *et al.*, Jpn. J. Appl. Phys., Part 1 **30**, 1102 (1991).
[9] K. Patorski, *Progress in Optics*, edited by E. Wolf (Elsevier Science, B. V., Amsterdam, 1989), Vol. XXVII, pp. 3–107.
[10] H. Weisen, Plasma Phys. Controlled Fusion **28**, 1147 (1986).
[11] L. N. Vycheslavov *et al.*, Proceedings of the 29th EPS Conference on PPCF, Montreux, 2002, P-5.105.
[12] J. Howard and L. E. Sharp, Plasma Phys. Controlled Fusion **34**, 1133 (1992).
[13] T. Akiyama, K. Tanaka, and L. N. Vyacheslavov, Rev. Sci. Instrum. (these proceedings).
[14] Focus Software, Incorporated
[15] S. Kado *et al.*, Jpn. J. Appl. Phys., Part 1 **34**, 6492 (1995).
[16] K. Tanaka *et al.*, J. Plasma Fusion Res. **4**, 427 (2001).
[17] H. Yamada *et al.*, Phys. Rev. Lett. **84**, 1216 (2000).
[18] S. Coda, M. Porkolab, and K. H. Burrel, Phys. Rev. Lett. **86**, 4835 (2001).
[19] L. E. Sharp, Plasma Phys. **25**, 781 (1983).
[20] K. Tanaka *et al.*, Rev. Sci. Instrum. **72**, 1089 (2001).